AIAA 2002-4536

Thermal Analysis and Correlation of the Mars Odyssey Spacecraft's Solar Array During Aerobraking Operations

John A. Dec, Joseph F. Gasbarre
NASA Langley Research Center
Hampton VA.

Benjamin E. George, 1Lt
United States Air Force, Kirkland AFB
Albuquerque, NM

AIAA/AAS Astrodynamics Conference
5-8 August 2002
Monterey, California

THERMAL ANALYSIS AND CORRELATION OF THE MARS ODYSSEY SPACECRAFT'S SOLAR ARRAY DURING AEROBRAKING OPERATIONS

John A. Dec and Joseph F. Gasbarre
National Aeronautics and Space Administration
Langley Research Center
Hampton, VA 23681-2199

Benjamin E. George, 1Lt
United States Air Force
Kirtland Air Force Base
Albuquerque, NM 87117

ABSTRACT

The Mars Odyssey spacecraft made use of multipass aerobraking to gradually reduce its orbit period from a highly elliptical insertion orbit to its final science orbit. Aerobraking operations provided an opportunity to apply advanced thermal analysis techniques to predict the temperature of the spacecraft's solar array for each drag pass. Odyssey telemetry data was used to correlate the thermal model. The thermal analysis was tightly coupled to the flight mechanics, aerodynamics, and atmospheric modeling efforts being performed during operations. Specifically, the thermal analysis predictions required a calculation of the spacecraft's velocity relative to the atmosphere, a prediction of the atmospheric density, and a prediction of the heat transfer coefficients due to aerodynamic heating. Temperature correlations were performed by comparing predicted temperatures of the thermocouples to the actual thermocouple readings from the spacecraft. Time histories of the spacecraft relative velocity, atmospheric density, and heat transfer coefficients, calculated using flight accelerometer and quaternion data, were used to calculate the aerodynamic heating. During aerobraking operations, the correlations were used to continually update the thermal model, thus increasing confidence in the predictions. This paper describes the thermal analysis that was performed and presents the correlations to the flight data.

INTRODUCTION

The Mars Odyssey spacecraft was launched on a Delta II launch vehicle from Cape Canaveral Air Force Station on April 7th 2001. On October 23rd 2001, after a 197-day cruise, the spacecraft performed a propulsive maneuver to insert itself into an 18.5-hour elliptic orbit around Mars. To place itself into its 2-hour, 400km circular, sun-synchronous mapping orbit, Odyssey used the multipass aerobraking technique, which was utilized by the Magellan spacecraft around Venus and the Mars Global Surveyor spacecraft around Mars. Aerobraking makes use of atmospheric drag on each orbit pass to gradually reduce a spacecraft's velocity at periapsis, which then reduces the altitude at apoapsis. The Magellan spacecraft was the first three-axis stabilized spacecraft to perform this type of multipass aerobraking.[1] Mars Global Surveyor, the second to use multipass aerobraking, gradually reduced its orbit from an elliptic 48-hour period to about a 380km 2-hour circular orbit.

To control periapsis altitude, Magellan planned on using thermocouple data to signal the need to perform a periapsis raise maneuver, which would raise the periapsis altitude, lower the maximum atmospheric density experienced, and thus lower the aerodynamic heating on the spacecraft and solar arrays. In the literature, it was noted that Magellan experienced at least 5 thermocouple failures prior to the start of aerobraking.[2] It is unclear from the available literature if any of these thermocouples were located on the solar arrays and were to be used during operations. It is also unclear whether or not there were any thermal models developed and used during the Magellan aerobraking process to make up for the inoperable thermocouples, but there are references to heat rate and surface temperature calculations being performed using a direct simulation Monte Carlo particle method.[3,4] In any event it is clear that in the early 1990's the limitations of computers would have prohibited the use of a detailed enough finite element or finite difference model that could have been run in a timely enough fashion to be used during operations. During the Mars Global Surveyor operations, the heat rate encountered

during previous drag passes was reconstructed using a 1-dimensional thermal model at various locations around the solar arrays. This model used the spacecraft and solar array thermocouple temperature data as input to determine what heat rate the spacecraft and solar arrays experienced. A thermal model to predict the solar array temperatures for future drag passes and to reconstruct the solar panel temperatures for past orbits was not available. Originally, during operations, the plan for Mars Odyssey was to use a 1-dimensional thermal model similar to that of the Mars Global Surveyor model. Unlike Magellan and Mars Global Surveyor, Mars Odyssey was the first multipass aerobraking mission to make use of detailed 3-dimensional finite element thermal model during operations to predict the temperatures for future orbits and reconstruct the solar panel temperatures for past orbits. This model, used in addition to the 1-dimensional model, provided detailed, 3-dimensional temperature profiles of the solar array, transient plots of maximum material temperatures, and transient plots of thermocouple temperatures. It also provided the ability to identify the hottest spots on the solar array, and provided a means to develop thermal limits based on heat rate or atmospheric density.

SOLAR ARRAY DESCRIPTION

The function of Mars Odyssey's solar array is two-fold. First, its primary function is to provide a stable power source for the spacecraft and scientific instruments during all phases of the mission. Second, while in the stowed configuration, the solar array provides a large surface area on which the aerodynamic forces can act during each drag pass of aerobraking. Following Mars orbit insertion the Odyssey spacecraft begins aerobraking by slicing through the Martian atmosphere at a relative velocity of about 4.57 km/s. Despite low atmospheric densities of about 80 kg/km^3, these high velocities, along with the large exposed surface area, produce significant aerodynamic heating on the solar array, and spacecraft. Careful design and construction of the solar array allows it to withstand this aerodynamic heating.[6]

The Mars Odyssey solar array is a three panel, layered construction of low density materials. The panels are commonly referred to as the +X, -X, and mid panels. The +X and –X panels are mirror images of each other, while the mid panel has a unique geometry. Figure 1 shows a 3-dimensional geometric representation of the solar array. This geometric representation was developed in MSC/PATRAN and was used in the aerobraking thermal analysis. Each panel consists of five layers; the first three make up the structural components and provide the structural integrity during launch and throughout aerobraking. Specifically, the solar array structure is a sandwich construction with a 0.190mm facesheet of M55J graphite composite, a 19.05mm aluminum honeycomb core, and another 0.190mm M55J composite facesheet.

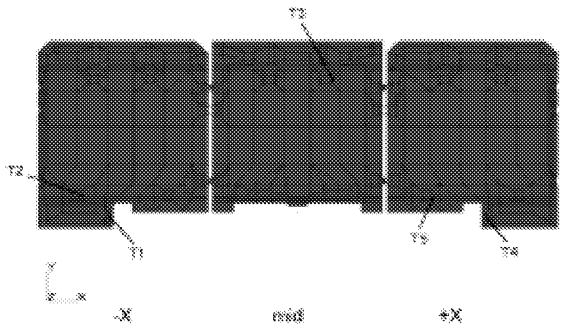

Figure 1. 3-D geometric representation of the Mars Odyssey solar array.

The next layer is a 0.051mm Kapton sheet that is co-cured to the M55J graphite beneath it. The next layer is the solar cell layer and is made up of several sublayers: 0.190mm Gallium Arsenide solar cells, 0.152mm cover glass, and 0.229mm of adhesives[6]. Figure 2 shows a cross-sectional view of the solar array at a represenatative location.

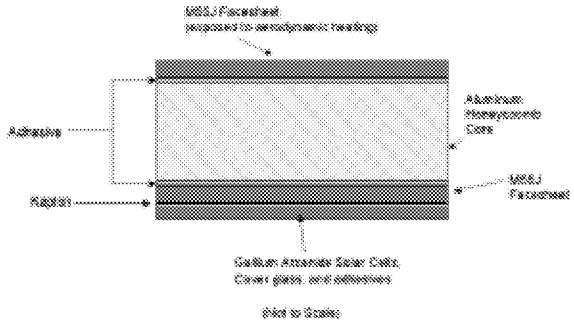

Figure 2. Cross-section of Mars Odyssey solar array

To reinforce certain areas of the array, sections of the standard 19.05mm thick, 1.0 lb/ft^3 aluminum honeycomb core were replaced with a higher density core of the same thickness. Also, to reinforce the array's hard points, a doubler sandwich structure was used. The doubler sandwich structure consisted of 0.381mm layers of M55J graphite composite on either side of a 18.161mm aluminum honeycomb core. The doubler core densities varied depending on the location within the array and the expected loading in the region of concern. Examples of such reinforced hard points on the array are the hinge mounting points. Overall, the

array design makes use of four different density aluminum honeycomb cores.

To protect the array from aerodynamic heating, a 0.072mm thick layer of multilayer insulation (MLI) was placed on the facesheet exposed to the aerodynamic heating and around the edges of the M55J graphite facesheet. The bulk of the MLI was on the facesheet surface, and a small portion wrapped around the edges and terminated on the solar cell side. The width of the MLI on the solar cell side ranged from 50 – 148mm.

The solar array has five thermocouples. There is one thermocouple on the mid panel on the solar cell side of the array. The +X and – X panels each have one thermocouple on the solar cell side and one on the "hot" facesheet side. On the engineering drawings[6], the thermocouples are designated T1, T2, T3, T4, and T5. T1 and T4 are on the +/-X panel on the exposed facesheet side. T2, T3, and T5 are on the solar cell side; Figure 1 shows the locations of the thermocouples on the array.

THERMAL MODELING

The thermal analysis of the solar array had three main components: the view factor and orbital heating analysis, the aerodynamic heating analysis, and the computation of solar array temperatures. The calculations were performed in two flight regimes. One regime was the vacuum phase where the spacecraft was in orbit around Mars, but out of the atmosphere. The thermal environment in this phase was dominated by the solar and planetary heating with negligible aerodynamic heating. The second regime was the aerobraking phase, or drag pass, where the spacecraft made its excursion into the atmosphere. The thermal environment in this phase was dominated by the aerodynamic heating with aerodynamic heating being roughly 60 times greater than the orbital heating. Temperatures were calculated for both flight regimes. Accurate calculation of the solar/planetary flux during flight, as well as aerodynamic heating during drag passes, requires that the thermal analysis be tightly coupled to the flight mechanics, aerodynamics, and atmospheric analysis. The orbital heating and view factor analysis, or radiation model, was developed using Thermal Desktop, a commercially available software package.[7] The radiation model was developed using engineering drawings of the spacecraft and solar array.[6] View factor and heat rate calculations were performed for several different solar array configurations and spacecraft orientations. First, calculations were made with the spacecraft and solar array in its vacuum phase configuration; the spacecraft oriented with its high gain antenna pointed towards Earth and the solar array normal to the sun. In transitioning to the aerobrake configuration, both heat rates and view factors to space for the solar array were calculated as the solar array articulated to its stowed position. As the spacecraft slewed to the aerobraking configuration, the solar array's view factors to space did not change, so view factors did not have to be recalculated for that maneuver.

Figures 3 and 4 show the spacecraft and solar array in the aerobrake configuration and vacuum phase respectively. This part of the analysis required detailed knowledge of the orbit and spacecraft orientation, and thus was highly dependent on the flight mechanics analysis.

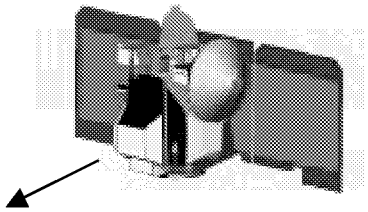

Figure 3. Mars Odyssey Thermal Desktop model in the aerobrake configuration.

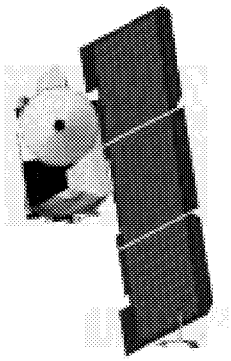

Figure 4. Mars Odyssey Thermal Desktop model in the vacuum phase configuration, view from Earth.

The aerodynamic heating analysis consisted of calculating the atmospheric density, the spacecraft velocity relative to the atmosphere, and the heating coefficient for points spatially across the array. Using this information, the incident aerodynamic heating was calculated using equation 1,

$$Q_i = \frac{1}{2} \cdot \rho \cdot V^3 \cdot C_H \qquad (1)$$

where ρ is the atmospheric density, V is the relative velocity, and C_H is the heat transfer coefficient. This calculation was made at 5 second intervals throughout the aerobraking pass to give a transient representation of aerodynamic heating. The flight mechanics team reconstructed the aerobraking pass and provided the relative velocity. The density and the heating coefficients were calculated using a Direct Simulation Monte Carlo (DSMC) particle method which allowed the density to be calculated using acceleration readings from the flight accelerometer and the heating coefficients to be calculated using the density and the relative atmospheric velocity. Due to the long run times needed to perform the DSMC computations, an aerothermodynamic database was developed prior to aerobraking. Then for each time step, the density was calculated by interpolating the accelerometer data, and the heating coefficients across the array were calculated by interpolating between density and relative velocity. The interpolation error on the heating coefficients was calculated to be about 2%, which was within the accuracy of the DSMC calculations. The heat transfer coefficients ranged from a peak value of 0.90 to a low value of 0, and included the surface accommodation coefficient. The model also accounts for reflected heat, which was approximated empirically for this mission using equation 2 and is a function of the incident heat flux and surface temperature.

$$Q_{ref} = \tfrac{1}{2}\rho V^3 \left[0.015 + 0.1\left(1 - \frac{Q_i}{\tfrac{1}{2}\rho V^3} \right) \right] \cdot \left(\frac{T_{wall}}{300} \right) \qquad (2)$$

where T_{wall} is the surface temperature of the solar array. Equations 1 and 2 reveal the coupling of the thermal analysis to the flight mechanics, aerodynamics and atmospheric analysis. These calculations provided an accurate representation of the aerodynamic heating as well as reflected heating that was a function of time as well as position on the solar array.

The temperatures for the solar array were calculated with the commercially available software MSC/PATRAN Thermal.[8] Like the Thermal Desktop model, the PATRAN Thermal model was developed solely using engineering drawings.[6] The model represented all three solar panels, and included both facesheet layers, the aluminum honeycomb core, the Kapton, the MLI, and one layer for the solar cells. The solar cell layer included the cover glass, wire, solder, and adhesives that were modeled as an averaged mass spread evenly across the layer. This was an engineering approximation since the wire, solder etc. were not evenly distributed across the panels. The titanium hinges and dampers that physically connect the three solar panels were also included in the model and provided a thermal link between the three panels. The model was highly detailed and included the variations in the aluminum honeycomb core density as well as the varying thickness of M55J composite doublers. For all materials, properties were included as functions of temperature; for the aluminum honeycomb core and M55J facesheets, orthotropic material properties were included. The five spacecraft thermocouples were modeled as bar elements which had mass and were thermally connected to the spacecraft with a contact resistance. Overall the PATRAN thermal model was a physically accurate 3D representation of the solar array. Compared to the as-built mass of the solar array of 32.3 kg, the mass of the PATRAN thermal model was 33.4 kg, a difference of only 3.4%.

The PATRAN thermal model required input boundary conditions from the two analysis components mentioned earlier. The model included radiation to space, incorporating the view factors that were calculated from Thermal Desktop. The orbital and planetary heat fluxes calculated from Thermal Desktop were applied to the surfaces of the model as well. The aerodynamic heating and reflected heating boundary conditions were applied to the exposed M55J facesheet and MLI surfaces. Heating on the edges of the panels was included as 5% of the incident heating of the nodes closest to the edge. Edge radiation was included around the outer-most edges with a view factor to space of 1.0. Radiation back to the spacecraft bus was included, with the spacecraft bus simply modeled as a node with a constant temperature. Initially this temperature was approximated using spacecraft temperature data for the trajectory correction maneuvers (TCM's), and then was updated using data from the first few orbit drag passes.

Steady state temperatures were calculated for the solar array in the vacuum phase prior to the start of the drag pass. As the spacecraft began to stow the solar array and slew into the aerobrake configuration, a transient analysis was made to obtain the initial temperatures at the start of the drag pass. The temperatures obtained prior to the drag pass were primarily dependent on the orbital heat rates and view factors calculated from Thermal Desktop, but most significantly, they were influenced by the fact that the spacecraft passed into solar occultation and was shaded by Mars on average, for about 4 minutes before the drag pass began. This reduced the initial temperatures and, allowed the solar array to absorb more energy and therefore increased the

margin between the flight temperatures and the thermal limits. Finally, during the drag pass, a transient analysis was performed to determine the temperatures, where the aerodynamic heating was dominant. Temperature predictions were made prior to each drag pass and temperatures were calculated using actual spacecraft telemetry to reconstruct past orbits.

A more complete discussion on the thermal analysis and the methodology used on the Mars Odyssey solar array can be found in a related publication.[9]

DRAG PASS AND TEMPERATURE PREDICTIONS

The initial goal of the thermal analysis was to provide an independent validation and verification of the analysis already being performed on the solar array. The high fidelity nature of this 3-dimensional analysis, and the speed at which analysis results could be produced, were compelling evidence to include this analysis in the trajectory decision making process during aerobraking operations.

The timeline for spacecraft maneuver decisions dictated the turn around time for analysis. Each day the drag pass temperature predictions as well as any reconstructed temperatures had to be completed by 12 noon eastern standard time. For the analysis to be useful during operations and be included in the Aerobraking Planning Group's (APG) maneuver decision-making process, it had to be generated efficiently. Utilizing a 1.7Ghz dual XEON processor computer made it possible for this highly detailed finite element analysis to run in about one hour. As the mission progressed, the duration of each drag pass increased. This caused the analysis run times to increase slightly but never caused them to exceed 1 hour 15 minutes. Computer speed alone was not the only means of increasing efficiency. The spacecraft's configuration in the vacuum phase was always the same so vacuum phase temperatures remained virtually constant. Also, the occultation duration changed very slowly, causing the initial temperatures to change at a slow, predictable rate. Therefore, to increase analysis efficiency, the view factor, orbital heating, and vacuum phase temperature analyses were performed on an as-needed basis.

The thermal analysis was highly dependent on all of the other analyses being performed. The thermal analysis took the longest to run and was always the last to be completed. Any problems arising within another group's analysis caused delays in the completion of the thermal analysis. Despite the tight operations schedule, the analysis generated a large quantity of information about the thermal state of the solar array. Figure 5 shows the predicted temperature distribution for orbit pass 40, just after periapsis, which is typical of the majority of the drag passes encountered. This temperature distribution was calculated using a predicted density, and velocity profile, and assumed a nominal orientation relative to the atmosphere. Figure 6 shows the predicted temperature of the thermocouples and the predicted heat rate as a function of time centered on periapsis. A similar transient plot was generated for each material, where the maximum predicted temperature for any location on that material is tracked. Figure 7 shows the maximum material temperatures as a function of time.

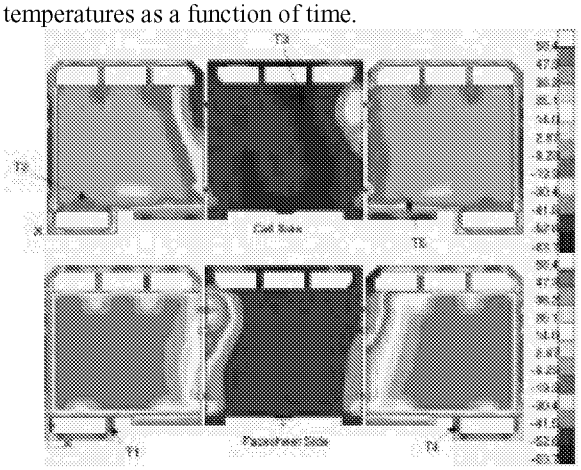

Figure 5. Predicted temperature distribution on the solar array for orbit pass 40.

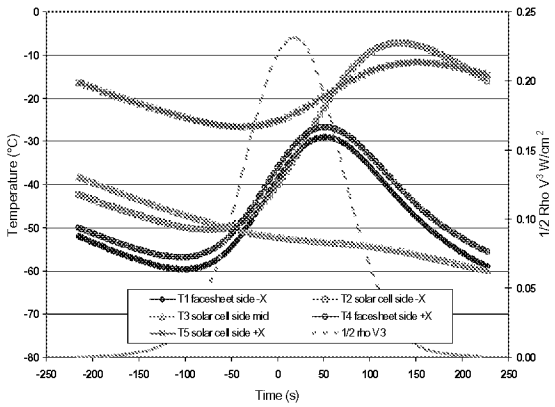

Figure 6. Thermocouple temperature predictions, orbit pass 040, peak heat flux = 0.232 W/cm^2.

This plot differs slightly from the plot of the thermocouple temperatures. The obvious difference is that the maximum material temperatures are significantly higher than the predicted thermocouple

temperatures. In the case of the M55J graphite, which was exposed to the flow, the figures show that the peak temperature was 85°C higher than the peak on either of the facesheet thermocouples, T1 and T4.

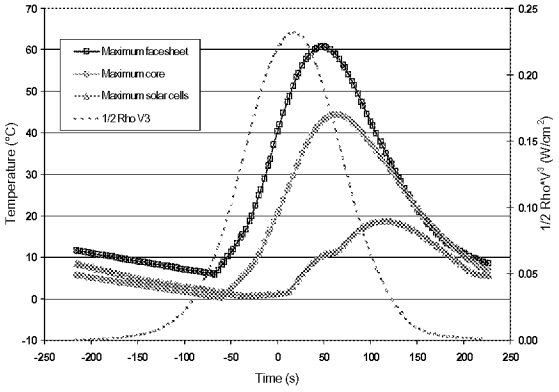

Figure 7. Maximum predicted material temperatures, orbit pass 040, peak heat flux = 0.232 W/cm^2.

This was a result of having MLI covering the facesheet in the areas near those thermocouples. The MLI provided sufficient shielding to the underlying material from the incident heat flux to prevent the material in those regions from reaching higher temperatures. Throughout the main phase of aerobraking, the magnitude of the temperature difference between the material maximum and the thermocouple maximum was dependent on the heat flux, and the difference grew as the magnitude of the heat flux grew. The material maximum was always higher than what the thermocouples indicated and was always located in the lower, outboard quadrant of the +X panel. Another minor difference between the thermocouple and maximum material plots is due to the fact that the location of the maximum material temperature changed throughout the pass. In Figure 7 where there seem to be discontinuities and the temperature seems to jump, the the maximum temperature shifts to another node in that particular material layer.

In Figures 6 and 7, the heat rate is represented by a smooth gaussian like profile. The heating is directly proportional to the atmospheric density; the density predictions, which came from an Odyssey version of Mars GRAM 2000, do not account for atmospheric density variations and thus have an average density profile as a function of altitude. Large uncertainties in predicting the atmospheric density from orbit to orbit made the temperature predictions less valuable than expected, but they were still useful in that they gave a 3-dimensional picture of the thermal state of the array, and could identify any thermal anomalies.

Although the uncertainties in the density predictions were present, they did not impact the prediction of the thermal limit lines, which turned out to be a very useful tool. The flight corridor for main phase aerobraking was chosen based on the maximum Q dot, which was the value of the aerodynamic heating that would cause the solar array to exceed its flight allowable temperature limit for the structure of 175°C. The upper flight corridor was reduced by a factor of 2 to carry 100% margin with respect to the limit. Figure 8 is a plot of the maximum solar array temperature as a function of Q dot, covering orbit passes 77 through 99. This plot was updated on a weekly basis by running the PATRAN thermal model with varying density and hence heating profiles. Four different density profiles were used: the low, middle, and upper ends of the flight corridor, as well as one that which would produce a maximum Q dot of 0.8 W/cm^2. A Q dot of 0.8 W/cm^2 was chosen as the upper bounding case because it guaranteed the solar array prediction would exceed the flight allowable temperature of 175°C. By using a predicted Q dot, or one derived from flight data, the JPL Navigation team could quickly determine the maximum predicted temperature of the solar array.

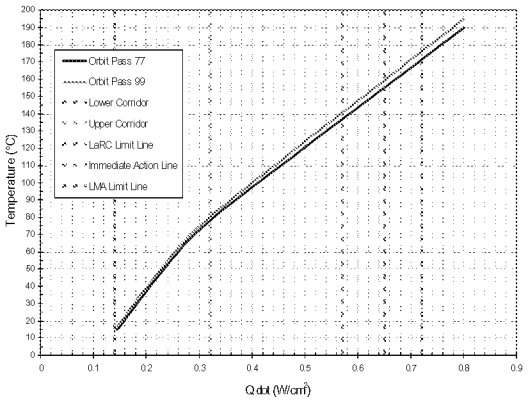

Figure 8. Temperature as a function of Q dot and orbit pass.

Determining the thermal limit of the solar array in terms of the Q dot was obtained simply by finding the value of Q dot that corresponded to 175°C. As the mission progressed the correlation of the thermal model to flight data improved significantly. Since the thermal model was updated continuously based on the correlations, confidence in the limit line chart increased dramatically. In figure 8 there are two limit lines: one is a limit line based on the NASA Langley 3-dimensional finite element thermal model, and the other is the limit line calculated by Lockheed Martin's 1-dimensional model of the solar array. The Lockheed limit line was more conservative and as such was used as the flight maximum.

TEMPERATURE CORRELATIONS TO FLIGHT DATA

For each orbit pass, the solar array temperatures were reconstructed using telemetry from the spacecraft. Comparing the temperatures calculated using the flight data with the spacecraft thermocouple data provided a means with which the thermal model's accuracy could be assessed. Moreover, since the thermal analysis was highly dependent on the other analysis being performed, the thermal model correlations could also be used to give an overall assessment of the aerobraking analysis process and assess the accuracy of the other analysis models.

The required inputs for the thermal reconstructions came largely from accelerometer data transmitted from the spacecraft. Once the data was in hand, the NASA Langley accelerometer team processed the data and obtained the atmospheric density and flight velocity. The aerodynamic heating was then calculated the same way as in the predictions, with the only difference being that the density and velocity profiles used were "real" instead of predicted. Vectors to the Sun and to Mars could also be obtained from this data and were used in the orbital heating component of the analysis. The time of periapsis could also be determined from the data and was used as the reference time for the plots.

For illustration purposes in this paper, orbit 106 is shown at various stages in the correlation process. Orbit 106 was chosen because it was the orbit which had the highest atmospheric density and hence the highest heat rate. The Q dot for orbit 106 peaked at 0.544 W/cm^2 and the solar array reached a maximum temperature of 136°C. Orbit 106 was reconstructed using the thermal model that was available at the beginning of aerobraking, the model that was current at the time orbit 106 was made, and with the final correlated model. At the beginning of aerobraking operations, the only data available was from the TCM's. This data was used as a starting point in correlating the model, but since the thermal environments were drastically different, it was not sufficient to allow full correlation of the model. Thus, the correlations for the first few aerobraking passes did not match the flight data very well. Figure 9 shows a transient plot of the flight thermocouple temperatures and the reconstructed thermocouple temperatures for orbit pass 106.

Looking at the plot, several statements can be made about the initial thermal model. First is that the time to reach the peak temperature in the thermal model lagged the flight thermocouple data. Second, the thermal model's peak temperature overshoots the flight data, providing a more conservative estimate. Third, the facesheet thermocouples in the model cooled down at a slower rate than the flight data. Finally, there was an initial temperature offset between the flight data and the thermal model.

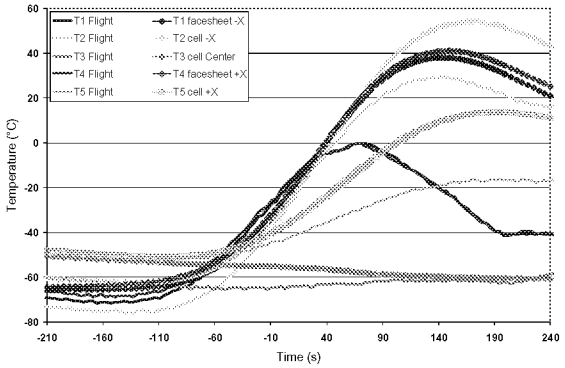

Figure 9. Reconstructed temperatures, orbit pass 106, using the initial uncorrelated thermal model.

The timing difference between the flight data and the model was affected by the way the thermocouples were represented in the thermal model. The thermal model was created using only drawings of the solar array, without detailed manufacturing knowledge. The exact mass of each thermocouple, as well as the amount of adhesive used to bond them to the solar array, was unknown. These parameters had to be approximated. In the thermal model these are simulated by a contact resistance to represent the bonded connection between the thermocouples and the array; and the density and cross-sectional area of the thermocouple bar element to simulate the mass. The mass of the thermocouple affects the speed with which it reacts to temperature changes and to some extent the peak temperature that it attains. The contact resistance affects the temperature difference between the bar element and material layer it is connected to, and thus affects the peak temperatures reached.

Looking back at Figure 5, the highest temperatures in the panel occur on the facesheet side, but directly behind these high temperature areas are the solar cell side thermocouples. In the model, too much heat from the facesheet side was being transferred to the solar cell side and down the "wings" to the areas near the facesheet thermocouples. Differences in the peak temperature magnitudes were primarily affected by two factors. The first was not including the reflected heat calculation initially, and second was the through panel conductance. Early on when the heat fluxes were still low, it was believed that the contribution of the reflected heat was insignificant, but this did not prove

to be the case. Including the reflected heat reduced the facesheet side temperature and reduced the amount of heat transferred to the solar cell side and down to the wings where T1 and T4 are located. Also, slight adjustments to the through panel conductance were made to help alleviate some of this transferred heat as well. The mid panel thermocouple, T3, was not exposed to the aerodynamic heating and thus its temperature did not change much. Aside from the initial temperature difference it was in good agreement with the flight data. The fact that T3 matched well indicated that the through the thickness conductance was consistent with the flight article, so adjustments to the conductance of the panels was minimal. It was not altogether intuitive, but the cool down performance of the facesheet thermocouples was affected by the assumed value of the effective emissivity (ε^*) between the MLI and the M55J facesheet. While the ε^* had its greatest effect on the facesheet thermocouples, T1 and T4, it also had a slight impact on the cell side thermocouples T2 and T5. Initially, in the absence of any test data, the effective emissivity was conservatively chosen as 0.1. After examining the flight data and running several cases varying the effective emissivity, an ε^* of 0.05 was found to best match the cool down.

Using data from orbits 005 through 020, a suitable correlation for the thermocouple mass and contact resistance was found. Also, the calculation for the reflected heat was included and the value for ε^* was updated. Figure 10 shows orbit pass 106 with these correlations applied.

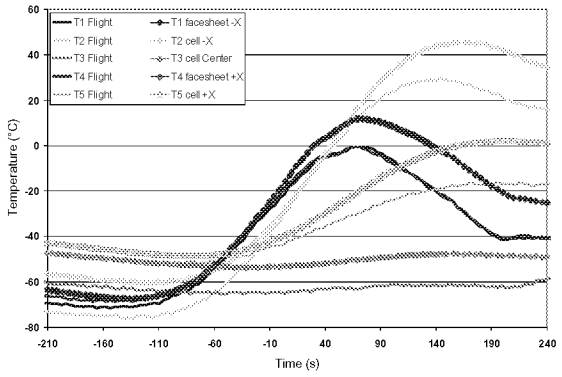

Figure 10. Reconstructed temperatures, orbit pass 106, using the partially correlated thermal model.

At this point in the correlation, the timing difference was minimized, the peak temperature overshoot was reduced, and the cool down performance had shown improvement. The cool down performance and the overshoot for T1 and T4 did improve but they were still at unacceptable levels. It was as if something in the flight article was impeding the heat flow to those thermocouples. There were three possible explanations. One was that since in the wing region the facesheet and aluminum honeycomb core are very narrow, there may have been a manufacturing flaw, or discontinuity in the material disrupting the heat flow, whereas in the thermal model each material layer was continuous. Second, during thermocouple installation, the thermocouples may not have been placed in exactly the same location as indicated in the drawings. In the thermal model, the thermocouples were placed as indicated on the drawings, this would definitely cause some disparity. Finally, in refining the model details, it was discovered that there was up to 6.35mm of syntactic foam packed around the edges of the aluminum honeycomb core in some regions. Syntactic foam has a very low conductivity and would impede heat flow in the regions where it was present. Figure 11 shows the wing region of the +X solar panel without the Kapton layer. To simulate the effects of the syntactic foam, the thermal conductivity of the nodes in the affected areas in the M55J facesheet and aluminum honeycomb core material were reduced and the density increased. These modifications were based on the simple rule of mixtures. Modifying the thermal conductivity and density in this way was done to expedite the inclusion of the syntactic foam and avoid addition of new solid geometry and additional finite element meshing in the model.

At this point the initial temperature error was still present. For the initial temperature error to be corrected, a temperature correlation in the vacuum phase up to the start of the drag pass was required. To accomplish this, a correlation coupling the Thermal

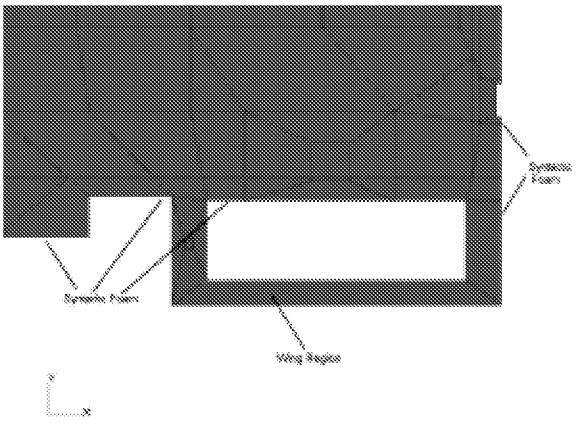

Figure 11. Close up view of +X panel wing region.

Desktop model and the PATRAN thermal model had to be developed. There were three main adjustments made to correlate the initial temperatures. First was the temperature assumed for the spacecraft in the PATRAN

model. Making adjustments to the spacecraft temperature also had a significant impact on the cool down rate for each of the thermocouples. The second and third adjustments were in the Thermal Desktop model. In the Thermal Desktop model the solar array is represented by 2-dimensional surfaces with two active sides. Initially it was felt that any solar or planetary flux that was incident in the third dimension, or edge on, would be insignificant. This turned out to be a bad assumption as there was a significant amount of flux on the inside edge of the wing regions near T1 and T4. Initially, to simplify the orbital heat flux calculations and reduce run time, specularity was not included. However, in order to increase the fidelity of the calculations, it was included. Including the specularity proved to be the missing element in the Thermal Desktop model and had the greatest impact on the initial temperature correlation. These adjustments as well as the adjustments made in correlating to the drag pass data were included in the model.

Figure 12 shows orbit pass 106 with all of the correlation adjustments applied. The mid panel thermocouple, T3, matches the flight data exactly. The difference between the facesheet thermocouples (T1 & T4) and the flight data was reduced to less than 10°C for the duration of the drag pass. There is still some overshoot error between the cell side thermocouples, T2 and T5. T3 matching the flight data as well as it does is an indication that overall, the through panel conductance was correlated very well. However, the local conductance near the cell side thermocouples T2 and T5 may have been slightly different. The solar cell side was modeled as a single, continuous layer of material.

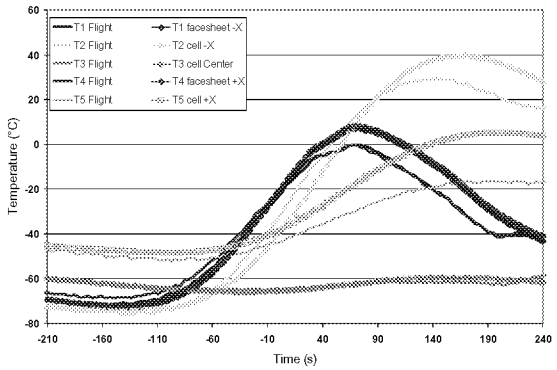

Figure 12. Recontructed temperatures, orbit pass 106, using the best correlated thermal model.

In reality, the solar array has wires, solder, and some spots where there are no solar cells. The thermocouples T2 and T5 are in regions that do not contain any solar cells, so they are mounted directly to the Kapton layer. Locally, there is less mass, and most significantly, lower solar absorptivity. Lower solar absorptivity in these local regions would reduce the amount of solar and planetary heat flux and thus reduce the temperature in these regions as observed in the flight data. The difference in local absorptivity was not modeled, but for future missions certainly should be.

As mentioned previously, Odyssey encountered the highest density of the mission on orbit pass 106, and hence this was the orbit pass with the largest aerodynamic heat flux. The higher heat flux intensified the effect of not including the local differences in solar heat flux. Looking at only orbit 106 can be deceiving because the differences between the flight data and the thermal model are maximized – in general, the differences throughout the mission were not this great. Table 1 summarizes the average differences in peak temperatures for each thermocouple at three different points during the main phase of aerobraking and gives the overall mission average. Taking a closer look at the temperatures over the entire drag pass, a root mean squared (RMS) average for each thermocouple over the duration of the drag pass was computed.

Table 1. Summary of peak temperature difference between the flight data and thermal model

	Average Peak Temperature Difference (°C)			
Sensor	Orbits 005 - 019	Orbits 020 - 095	Orbits 096 - 225	Mission Average
T1	4.1	3.1	2.1	2.90
T2	3.2	1.7	4.6	2.97
T3	0.1	0.2	0.2	0.16
T4	3.8	3.6	3.3	3.47
T5	6.5	6.9	9.2	7.53

Table 2 shows the RMS average for each thermocouple at three points during the main phase of aerobraking.

Table 2. Summary of RMS temperature differences between the flight data and thermal model

	RMS Temperature Difference (°C)			
Sensor	Orbits 005 - 019	Orbits 020 - 095	Orbits 096 - 225	Mission Average
T1	7.2	6.2	4.3	5.90
T2	4.6	4.1	5.4	4.70
T3	2.0	3.1	1.9	2.33
T4	6.9	6.5	5.6	6.33
T5	3.9	3.7	5.7	4.43

The RMS average provides a somewhat better means with which to assess how close the model was coming to the flight data for the duration of each drag pass and

also gives some insight into the progression of the correlation over the mission. Table 1 shows that for the most part, the thermal model matched the peak flight thermocouple temperatures quite well – usually within 3°C. Table 2 shows that when you look at the entire transient, the thermal model still matches the flight data extremely well, albeit not as well as only comparing the peak temperatures. Combining all of the thermocouples into one average, the average difference in the peak temperatures over the entire mission was 3.4°C. The average RMS temperature difference over the entire mission was 5.0°C.

The correlation of the thermal model was important for several reasons. The first is that correlating the thermal model gave an overall snapshot of the entire aerobraking analysis process and how well each of the different disciplines' analysis models were performing. In addition, correlating the thermal model gave confidence that the prediction of the thermal limit lines and the weekly Q dot versus temperature curve was accurate.

CONCLUSIONS

It has been shown that a 3-dimensional finite element model developed to represent the actual flight hardware can be used in an operational environment with great speed and accuracy. The detail captured and the quantity of data generated by such a high fidelity model is not possible using a 1-dimensional model alone. The 3-dimensional model showed that the hot spots were not located near any of the flight thermocouples. It is believed that such a high fidelity model, used earlier in the design phase, could identify the hot spots and be used to place thermocouples where they are most needed. Also, the 3-dimensional model demonstrated that it could be used to evaluate the thermal limit lines for the solar array in both the design and operational phases. Comparison to the flight data shows that over the entire mission, the thermal model performed extremely well. On average, the model did not exceed a 10°C difference in peak temperature, and over the duration of each drag pass the RMS temperature difference never exceeded 8°C. A fully correlated thermal model provides confidence in the analysis and eases the tension in the trajectory decision-making process.

ACKNOWLEDGMENTS

The authors would like to thank Ruth Amundsen for her thermal analysis and methods development on MGS which paved the way for the work done on Odyssey. Also, thanks go out to the JPL navigation team for giving us the opportunity to make a contribution to this mission. We would also like to thank Mike Lindell for providing supporting structural analysis.

REFERENCES

[1]Carpenter, A. S., "The Magellan Aerobraking Experiment: Attitude Control Simulation and Preliminary Flight Results", AIAA Paper 93-3830, August 1993.

[2]Neuman, J. C., Buescher, J. A., and Esterl, G. J., "Magellan Spacecraft Thermal Control System Design and Performance", AIAA 28th Thermophysics Conference, Orlando, Florida, AIAA 93-2844, July 6-9, 1993.

[3]Haas, B. L., Feiereisen, W. J., "Particle Simulation of Rarefied Aeropass Maneuvers of the Magellan Spacecraft", AIAA 27th Thermophysics Conference, Nashville, Tennessee, AIAA 92-2923, July 6-8, 1992.

[4]Haas, B. L., Schmitt, D. A., "Simulated Rarefied Aerodynamics of the Magellan Spacecraft During Aerobraking", AIAA 93-3676-CP, July 6-9, 1993.

[5]Beerer, J., et. al., "Aerobraking at Mars: The MGS Mission", AIAA 34th Aerospace Sciences Meeting and Exhibit, Reno, Nevada, AIAA 96-0334, January 15-18, 1996.

[6]Engineering Drawings from Lockheed Martin (919M0000020), SpectroLab Inc. (041312-041314), and Spectrum Astro Inc. (AM 111372-001, -002, -003) Various release dates 1997-1998.

[7]Thermal Desktop User's Manual, Version 4.4, Cullimore & Ring Technologies.

[8]MSC/PATRAN Thermal User's Guide, Version 2000r2 MSC Software.

[9]Dec, J.A., Amundsen, R. M., "A Thermal Analysis Approach for the Mars Odyssey Spacecraft's Solar Array", Proposed paper for the AIAA 36th Thermophysics Conference, Orlando, Florida, June 23-26, 2003.